Birefringence in the transparency region of GaAs/AlAs multiple quantum wells

A. A. Sirenko
Department of Physics, the Pennsylvania State University, University Park, Pennsylvania 16802

P. Etchegoin and A. Fainstein
Centro Atómico Bariloche and Instituto Balseiro, Comisión Nacional de Energía Atómica and Universidad Nacional de Cuyo, 8400-San Carlos de Bariloche, Río Negro, Argentina

K. Eberl and M. Cardona
Max-Planck-Institut für Festkörperforschung, Heisenbergstraße 1, D-70569 Stuttgart, Germany
(Received 1 March 1999)

Birefringence measurements for in-plane propagation of light below the absorption edge in GaAs/AlAs multiple quantum wells (MQW's) are reported for different well/barrier widths. A remarkable drop in the low-frequency limit of the birefringence has been observed for MQW structures with small periods and ascribed to the presence of local fields. The temperature dependence of the birefringence is also studied and complementary results in InP quantum dot structures are also presented. The latter exhibit a strong resonant birefringence, which can be explained by the reduced dimensionality in the joint density of states for optical transitions in the dots. [S0163-1829(99)00635-9]

I. INTRODUCTION

As the size of semiconductors is reduced in one or more dimensions to the nanoscale level, the otherwise isotropic bulk optical properties are modified. For quantum well (QW) structures based on III-V zinc-blende semiconductors and grown along a [001] direction, the original cubic T_d point group of the bulk is reduced to D_{2d} and the system becomes uniaxial. This reduction in symmetry results in an optical anisotropy (birefringence), which has been studied in QW structures using various experimental optical techniques such as absorption,[1–3] photoluminescence,[4] time of flight spectroscopy,[5] microscopic reflectance-difference spectroscopy,[6] and linear birefringence.[7] These methods yield a difference between the two principal components of the refractive index, $n_\perp$ and $n_\parallel$, for electromagnetic waves polarized in plane and along the QW-growth direction ($\hat{z}$), respectively. Both $n_\parallel$ and $n_\perp$ depend on the frequency of the light ω and they show a resonant dispersion when approaching a direct gap from below (as expected from the linear dispersion theory of the dielectric function).[8]

Previous studies of the linear birefringence in GaAs/AlAs multiple quantum wells (MQW's),[7,9] show that it is possible to measure the polarization state of the transmitted light for *in-plane* propagation, i.e., $\vec{k}_{light} \perp \hat{z}$. These structures were sandwiched between two cladding layers of a $Ga_{0.3}Al_{0.7}As$ alloy with an average index of refraction smaller than both, $n_\perp$ and $n_\parallel$, rendering a waveguide for in-plane propagation and producing an effective coupling of the light with the MQW's. The spectral range for these experiments is limited to the window between the optical gaps of the MQW's and that of the GaAs substrate[7,9] and this is, in fact, where resonant effects are expected to be most pronounced in the dispersion of the birefringence in view of the proximity of the absorption edge. In Refs. 7 and 9, it was suggested that the birefringence may change in MQW's with different well/barrier widths and it was shown that the main contribution to the resonant part of the birefringence is determined by the splitting of the light-(lh) and heavy-hole (hh) valence subbands. Moreover, it has been shown[9] that the application of uniaxial stress along $\hat{z}$ reduces the birefringence due to changes in the lh-hh splitting, demonstrating a direct competition between confinement and external stress. In this paper, we report on a systematic study of the birefringence in GaAs/AlAs MQW's with different periods (well + barrier widths) and, accordingly, with different splittings between the lh and hh valence subbands. The paper aims to answer a few very basic aspects of the linear optical properties of MQW's. Among them, the long wavelength (low energy) limit of the birefringence and the effect of resonant contributions to the dispersion from the different confined states are specifically examined.

In bulk semiconductors, it is well known[8] that the dielectric function in the transparency region has contributions that can be separated into: (i) a constant dispersionless background arising from high-energy gaps (Penn-gap contribution) and, (ii) a resonant term with the first dipole-allowed direct transition from the valence to the conduction band. The relative importance of the latter depends not only on its oscillator strength, but also on the critical point dimensionality in the joint density of states (JDOS). A material that has an anisotropic dielectric tensor is said to be *birefringent*. Zinc-blende semiconductors are not anisotropic by themselves, but they may become birefringent upon application of uniaxial stress.[8,10] In contrast, MQW's are intrinsically uniaxial due to their layered structure. In this case, the resonant contribution to the birefringence in the transparency region comes essentially from transitions between the confined hh and lh states and the conduction electron levels in the wells. The birefringence is a natural consequence of the different coupling of the hh- and lh-interband transitions with

the electric field of the light for polarizations either parallel or perpendicular to the plane of the MQW's, respectively.[7] As in bulk semiconductors, all other transitions to higher energy bands can be considered part of the so-called Penn gap. Moreover, the fact that MQW's have layers (where boundary conditions for the electric field of the light $\vec{E}$ must be satisfied) implies an additional contribution from *local fields* to the optical properties. Local fields result from the self-action of the electromagnetic field through the polarizability of the medium. In the bulk, local fields produce very small corrections to the dielectric properties, which must be obtained from the full band-structure.[11] In MQW's, however,[12] boundary conditions at the different layers play a significant role. Indeed, in the framework of a simple effective medium approach, this contribution to the birefringence is given by[12]

$$\Delta n=(\epsilon_{\perp}^{0})^{1/2}-(\epsilon_{\parallel}^{0})^{1/2}=\langle\epsilon^{0}\rangle^{1/2}-\langle 1/\epsilon^{0}\rangle^{-1/2}, \qquad (1)$$

where ϵ^0 indicates $\epsilon(\omega=0)$, and $\langle..\rangle$ represents the compositional average of the dielectric functions (or their inverses) of bulk GaAs and AlAs.[6,7] This effective medium estimate for Δn is independent of the MQW period for a fixed well/barrier ratio. The full microscopic calculation of local fields, however, implies the inversion of an infinite matrix with off-diagonal elements that depend on the reciprocal lattice vectors $\vec{G}$ of the periodic structure.[13] These off-diagonal matrix elements are, fortunately, small in bulk semiconductors and can be neglected for practical purposes. On the other hand, such local-field corrections in MQW's may not only give a sizable contribution but should also depend on the period. Such a calculation has not been performed to date due to stringent computer memory and time requirements.

In this paper we present a detailed study of the birefringence in the transparency region of MQW's with varying periods (for a fixed well/barrier thickness ratio). The underlying strategy is to evaluate the different contributions to the birefringence from the resonant- and Penn-gap-like transitions and discern whether local-field effects can be identified. The effects of temperature on the birefringence of MQW's and, in addition, the role of the reduced dimensionality in samples with InP-quantum dots (QD's), will also be illustrated.

The paper is organized as follows: Sec. II gives a few details of the samples and experimental methods, Sec. III presents the results with the necessary theoretical background for their interpretation while in Sec. IV a few conclusions are drawn.

II. EXPERIMENT

Structures with GaAs/AlAs MQW's were grown by molecular-beam epitaxy (MBE) on (001) GaAs substrates. Samples with symmetric GaAs wells/AlAs barriers of 20/20, 30/30, 40/40, 50/50, 60/60, and 70/70 Å have been studied. We identify the samples by these numbers hereafter. After Refs. 7 and 9, the MQW's were confined between two $Al_{0.7}Ga_{0.3}As$ layers of $\sim 1.5\,\mu$m each, producing a waveguiding effect for propagation along the planes ($\vec{k}_{light}\perp\hat{z}$). Notwithstanding, the MQW's themselves were made thick enough (about 1.2 μm along $\hat{z}$) to minimize the waveguide-induced birefringence with respect to the intrinsic birefringence of the MQW's.[7]

We also studied a structure with InP QD's grown by MBE on a (001) GaAs substrate in order to contrast and compare with the GaAs/AlAs MQW's. This sample contained a single layer of InP QD's symmetrically placed in an $In_{0.48}Ga_{0.52}P$ matrix, lattice matched to GaAs, with a total thickness of 0.13 μm. The average amount of InP in a single QD layer is equivalent to a uniform coverage of 3.0 monolayers. The average QD size is approximately 3 nm in height and 16 nm in base length, with a dot concentration of $\sim 5\times 10^{10}$ cm^{-2}. The $In_{0.48}Ga_{0.52}P$ matrix containing the QD's was surrounded by two 1 μm-thick $In_{0.48}Al_{0.52}P$ clad layers. The growth and optical properties of the InP QD structures are described in detail in Refs. 14–16.

The in-plane uniformity of the samples (inhomogeneous broadening) was monitored by means of photoluminescence spectroscopy. Samples with parallel opposite surfaces were prepared by cleaving and their length was $d\simeq 1$ mm in the [110]-direction, along which light is transmitted. For reasons that will become evident later, wedge samples with variable lengths d were also prepared by mechanical polishing. The angle between two opposite surfaces was about 1° as determined by means of both a profilimeter and an optical goniometer.

The birefringence for the different samples was obtained from the in-plane transmission of the white-light of a halogen-lamp detected with either a SPEX-1404 double monochromator or a DILOR-spectrometer equipped with a photomultiplier and a charge coupled device detector, respectively (see Refs. 7 and 9 for additional details). Spectra were obtained at both room (RT) and liquid helium temperatures in the energy window spanned by the fundamental gap of the GaAs substrate (~ 1.38 eV at 300 K) and that of the MQW's, which varies with the well-widths according to the different confinements. Transmission measurements were performed with two linear-crossed polarizers, oriented at 45° with respect to the MQW's $\hat{z}$ axis to minimize stray light.

III. RESULTS AND DISCUSSION

A. Dependence of $\Delta n(\omega)$ on the MQW period

Figure 1 shows the in-plane crossed-polarized transmission spectra for three of the aforementioned GaAs/AlAs MQW's together with the photoluminescence (PL) spectra obtained from the front face of the samples. For smaller well widths, the birefringence oscillations vanish at higher photon energies, evidencing the larger electronic gaps produced by confinement. The overshoot at ~ 1.385 eV seen in the 50/50 sample corresponds to the gap of the GaAs substrate.[7,9] Hence, no information about the birefringence of the MQW's can be gained below this energy. The incident light beam with $\vec{k}_{light}\|[110]$ and polarization at 45° with respect to $\hat{z}$ can be decomposed into two in-phase polarized electromagnetic waves along $\hat{x}'=[1\bar{1}0]$ and $\hat{z}=[001]$, respectively. The oscillations in Fig. 1 result from the phase difference between these two waves at the output face of the sample, acquired by the presence of the birefringence

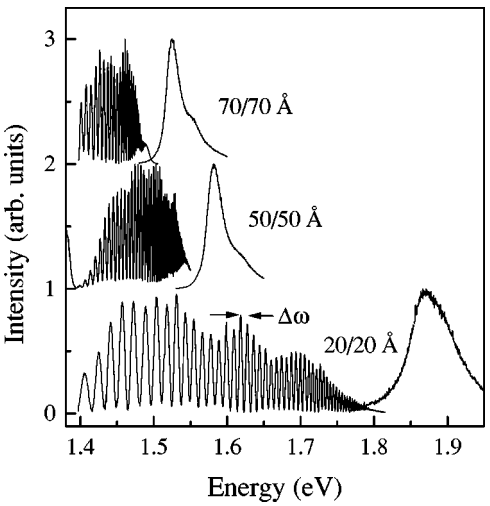

FIG. 1. In-plane transmission through crossed polarizers for samples with $d=1$ mm and different well/barrier widths shown next to the spectra. The birefringence oscillations disappear at the gaps of the MQW's which, owing to the different confinements, shift to higher energies for structures with smaller periods. The normalized PL spectra, measured from the upper face of the structures are also displayed. See the text for further details.

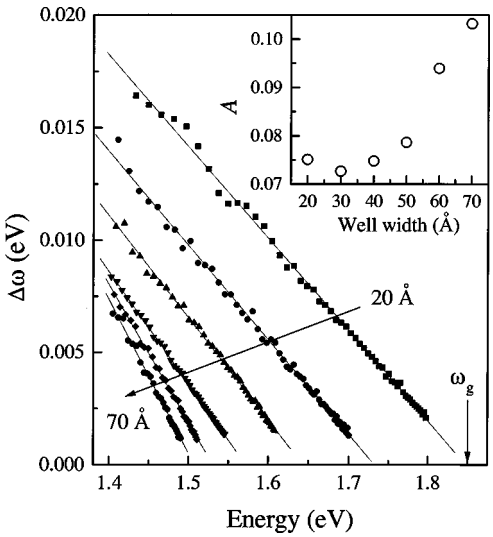

FIG. 2. Distance between fringes $\Delta\omega$ measured for MQW's with different well/barrier thicknesses (see Fig. 1). Solid lines represent linear fits to the experimental dependences: $\Delta\omega=A(\omega_g-\omega)$. A vertical arrow marks the gap ω_g of the 20/20 sample. The inset shows the variation of the parameter A vs well width.

$\Delta n=(n_\perp-n_\parallel)$. The maxima in the spectra are determined by the requirement that this phase difference should be equal to an integer multiple M of λ (Ref. 17)

$$\Delta n(\lambda)d=M\lambda, \tag{2}$$

where $\lambda=2\pi c/\omega$ is the wavelength of the light in vacuum. The crossed-polarized transmitted intensity in Fig. 1 is expected to be represented by[7,9]

$$I(\omega)\sim\sin^2\left[\frac{d}{2c}\Delta n(\omega)\omega\right]. \tag{3}$$

It should also be observed that it is impossible to obtain the sign of the birefringence from the spectra represented by Eq. (3) in Fig. 1. Nevertheless, it is known from previous studies[7] that $(n_\perp-n_\parallel)>0$. Equation (2) does not yield directly the value of $\Delta n(\omega)$, for M ($M\gg1$) is unknown. Had we used the experimental situation where *all* fringes [down to the first one with $M=1$, for which $\Delta n(\omega)d\sim2\pi c/\omega$] could be measured at very low frequencies, Eq. (2) would be used to determine the full dispersion of $\Delta n(\omega)$. The lowest energy accessible in the experiment is, nevertheless, limited by the gap of the GaAs substrate. We rewrite Eq. (2) in the following form:

$$\Delta n(\omega)=\frac{1}{\omega}\left[\Delta n^0\omega_0+\frac{2\pi c}{d}\int_{\omega_0}^{\omega}\frac{1}{\Delta\omega(x)}dx\right], \tag{4}$$

where $\Delta\omega(\omega)$ is the distance between fringes (see Fig. 2), which can be obtained from the experimental spectra shown in Fig. 1, and Δn^0 is the value of Δn at a reference frequency ω_0. The determination of Δn^0 will be described later. To facilitate the analysis of the experimental data, we replaced in Eq. (4) discrete by continuous functions and summation by integration, which is possible since $\Delta n(\omega)$ is expected to be a well behaved, dense, and smooth function of ω. The integral in Eq. (4) gives the number of fringes in the spectral range between ω_0 and ω.

It is clear from Eq. (4) that, in order to obtain the dispersion of $\Delta n(\omega)$, we need at least one calibration point for Δn^0 at ω_0. This is equivalent to the determination of the specific M in Eq. (2) corresponding to ω_0. In a previous study,[9] an independent determination of Δn at specific frequencies obtained with microscopic reflectance-difference spectroscopy[6] was used as calibration. Still, it is also possible to obtain a calibration value by way of transmission experiments between crossed polarizers only. This is where the wedge samples with variable d's come into play. Changes in d result in intensity variations described by Eq. (3). If d is varied by a known value δd, so that $\Delta n^0\delta d=2\pi c/\omega_0$, Δn^0 can be determined inasmuch as it corresponds to a phase shift of π in $I(\omega)$. To this end, the wedge samples were continuously displaced with the misoriented opposite surfaces in the direction perpendicular to both, $\vec{k}_{light}$ and the entrance slit of the spectrometer. As a result, we were able to probe different parts of the same structure with continuously varied values of d. Note that the value of Δn^0 depends only on the accuracy of δd which, in turn, is defined by the angle between the two surfaces of the sample and by the accuracy of the linear displacement with respect to the fixed entrance slit of the spectrometer. Figure 3 displays the experimental dependence for the phase shift in $I(\omega)$ and the raw transmission spectra for three close thicknesses. In principle, the full dispersion of $\Delta n(\omega)$ could be measured by this procedure, but in practice this procedure is extremely cumbersome, time-consuming, and less accurate close to the gap of the MQW's where the fringe-density significantly increases. Alternatively, we measured three values of Δn^0 at different ω_0's for each sample and use them as input parameters in Eq. (4). The birefringences so obtained are shown in Fig. 4 for MQW's with different periods. For all samples, Δn increases when the energy approaches the fundamental gap of the structures (shown by the vertical dashed lines). The curve

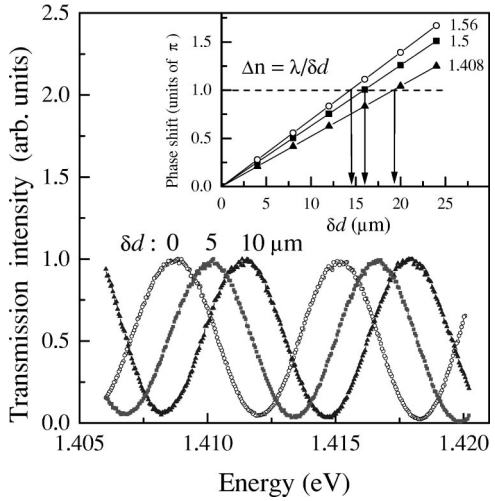

FIG. 3. Transmission spectra measured in the 40/40-Å sample for different d's. Note the shift of the fringes caused by a δd of 5 and 10 μm. The inset shows a linear fit to the experimental values of the phase, which allows for the determination of the value of δd resulting in the phase shift of π. The phase shift has been measured for three different energies shown next to the lines: 1.408, 1.5, and 1.56 eV. The change in the slope corresponds to an increase of the birefringence when energy changes from 1.408 to 1.56 eV.

for the 50/50 sample is very close to that reported in Ref. 9 for a thicker 50/50 MQW structure (2.8 μm). This demonstrates that the influence of the waveguide on the birefringence is negligible in our structures.

The implications of the introduction of Eq. (4) in the data analysis can be demonstrated as follows: we found that in all investigated structures with $d=1$ mm, the functions describing the distance between fringes $\Delta\omega(\omega)$ can be interpolated, in all or most of the measured energy range, by a simple linear expressions of the form $\Delta\omega(\omega)=A(\omega_g-\omega)$. These fits are shown in Fig. 2 together with the experimental data. Thus, by integrating Eq. (4) we can find an approximate expression for the birefringence in MQW's in the frequency range close to the resonance with the fundamental gap, to wit

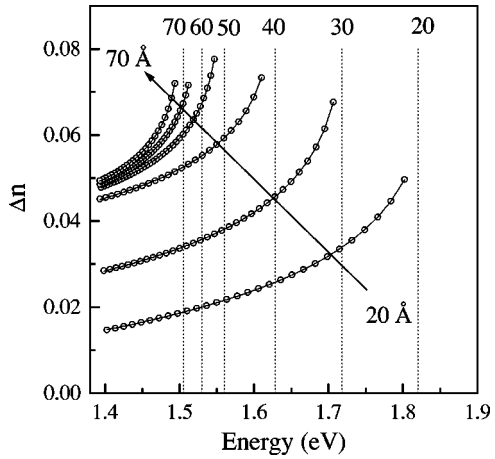

FIG. 4. Experimental birefringence dispersions (symbols) in MQW's with different periods. Solid lines represent fits to the experimental points with Eq. (6). The position of the electronic average gaps obtained from the fits are shown with dashed vertical lines.

$$\Delta n(\omega)=\Delta n^0\frac{\omega_0}{\omega}+\frac{\Omega}{\omega}\ln\frac{\omega_g-\omega_0}{\omega_g-\omega}. \tag{5}$$

Here, ω_g corresponds to the absorption gap which is close to the average between the lh and hh valence to conduction band transitions of the structure, Δn^0 is a calibration value at ω_0 ($\omega_0<\omega_g$), and $\Omega=2\pi c/Ad$ is the empirically determined parameter, which is independent on d since A scales as $1/d$. Note that the linear behavior observed for $\Delta\omega$ produces upon integration of Eq. (4) the logarithmic resonance behavior in $\Delta n(\omega)$ expected for a two-dimensional (2D) singularity in the JDOS.[8] On the other hand, the parameter Ω obtained from the fits continuously increases from 0.012 to 0.017 eV/$\hbar$ (see Fig. 2) for well widths varying from 70 to 30 Å , respectively. This implies a strengthening of the resonant contribution to the birefringence for narrow wells, as is expected from the confinement-induced increasing hh-lh splitting. It can also be observed in Fig. 2 that there is a sort of saturation in the value of A for well widths below 30 Å. This will be discussed below.

Besides being an empirical demonstration of the 2D nature of the MQW's JDOS, Eq. (5) represents a convenient way to express $\Delta n(\omega)$ near ω_g in terms of quantities (Ω, Δn^0, and ω_g) which can be determined experimentally. On the other hand, Eq. (5) only holds in the energy range where the linear fits in Fig. 2 are valid, and consequently it may not properly describe $\Delta n(\omega)$ for $\omega\rightarrow 0$ where the correctness of the linear approximation for $\Delta\omega$ cannot be experimentally verified. Moreover, Eq. (5) partly mixes the contribution of the Penn and direct gaps in the two terms. In fact, once the experimental dispersions are obtained, the data can be physically best described by[7]

$$\Delta n(\omega)=\Delta n_{bg}-\Delta n_{gap}\ \ln\left[1-\left(\frac{\omega}{\omega_g}\right)^2\right], \tag{6}$$

where the first and second terms represent the aforementioned background contribution (which in bulk samples comes from the Penn gap) and the logarithmic singularity with the direct gap, respectively. The dispersions for the different samples, which agree with Eq. (5) in the experimental range, will be fitted by Eq. (6) which explicitly separates the contributions we wish to extract from $\Delta n(\omega)$. Equation (6) is, of course, valid in the full energy range down to $\omega\rightarrow 0$ (except possible anomalies around the phonon frequencies) and constitutes a textbook example of birefringence in the transparency region for a solid with a 2D singularity in the lowest direct gap.[8] In Fig. 4, these fits are shown by solid lines together with the data. The agreement with the simple model of Eq. (6) is certainly remarkable. The vertical dashed lines in Fig. 4 are the gaps ω_g obtained from the fits, which coincide within $\sim$0.2% with the gaps determined by the linear extrapolation in Fig. 2.

The principal characteristics of the data in Fig. 4 can be summarized as follows: (i) there is a resonant increase of $\Delta n(\omega)$ when the gap is approached from below, (ii) the energy window spanned by the data increases with decreasing well widths (as expected from the different confinements) and, (iii) a strong decrease in the overall magnitude of $\Delta n(\omega)$ is observed for the thinner wells. These qualitative observations can be immediately put on quantitative grounds

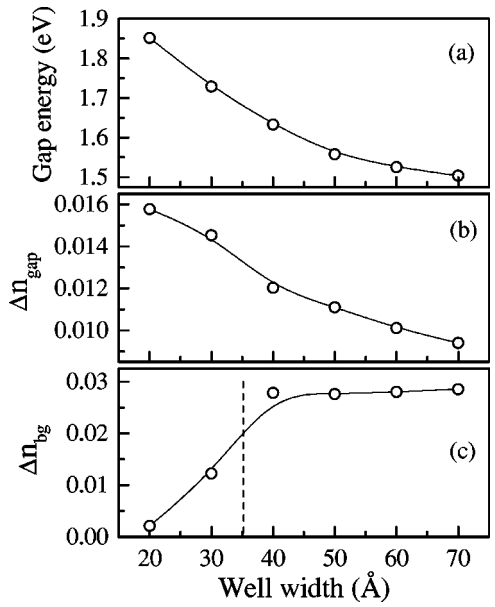

FIG. 5. Parameter of Eq. (6) vs well widths: (a) $\hbar\omega_g$, (b) Δn_{gap}, and (c) Δn_{bg}. Note the strong decrease of Δn_{bg} in the 20/20 and 30/30 samples. The solid lines are a guide to the eye. The vertical dashed line in (c) represents the transition between type-I and -II MQW's. See the text for further details.

through the parameters obtained from the fits with Eq. (6), which are displayed in Fig. 5. Figure 5(a) shows the expected continuous increase of the gap energies ω_g with decreasing well widths. Moreover, Δn_{gap} in Fig. 5(b) [as Ω in Eq. (5)] shows an increase of the strength of the resonance for thinner wells. As discussed above, this magnitude is basically determined by the hh-lh splitting. This splitting increases with confinement but saturates for small well widths. This saturation could explain the change in behavior of both A and Δn_{bg} in Figs. 2 and 5(b), respectively, for well widths below 35 Å. On the other hand, the sudden decrease of the background birefringence [represented by Δn_{bg} in Fig. 5(c)] for well widths below 40 Å lacks a straightforward interpretation. We conjecture that it is due to the presence of *local fields*, as we shall explain in what follows.

It is important to stress again at this point that the fits with Eq. (6) automatically decouple the effect of the resonant gap from Δn_{bg}. We believe the data in Fig. 5(c) cannot be attributed to a deficiency of the model or a coupling of the fitting parameters in Eq. (6). In fact, other models for the contributions of the singularity and the background birefringence give slightly different absolute values for Δn_{bg} but the qualitative picture remains unchanged. In addition we could avoid using an explicit model and obtain the same qualitative result directly from the experiment. For example, the data in Fig. 4 could be shifted so that the gaps coincide and we can compare the values of the birefringence at a fixed frequency (normally the lowest available). In this manner, the values for Δn_{bg} differ from the data in Fig. 5(c), but the relative drop for well widths below 35 Å remains. We considered three possible origins for the anomalous behavior of the birefringence background Δn_{bg}, namely: (i) the possible effect of the direct-to-indirect gap transition of MQW's with wells thinner than $\sim$35 Å, (ii) the effect of band folding on the high-energy transitions and, (iii) the presence of local fields.

It is well known[18] that in GaAs/AlAs MQW's, the crossover between direct and indirect gaps takes place for wells with widths $\sim$35 Å. For thinner wells, the X point becomes the lowest electronic state in the conduction band. This so-called type I-II transition revealed itself in our measurements also by a significant decrease in the PL intensity for the 20/20 and 30/30 structures. However, changes in the birefringence cannot be attributed to this crossover because the dielectric function still arises largely from direct vertical transitions, even when the minimum of the conduction band is at a different position than Γ as in bulk Si and Ge.[19] Although phonon-assisted optical transitions are possible at the indirect gap and in 20/20 and 30/30 samples they result in an absorption edge at ω_g, the indirect X-Γ gap has no practical effects for the description of the optical constants in the transparency region due to the negligibly small value of the matrix element.

The possible effect of band folding on the high-energy transition [point (ii) above] can also be discarded as the reason for the change in Δn_{bg}. The proof is simple and relies on the approximate sum rule for the dielectric function $\epsilon(\omega)$ of insulators at $\omega\sim 0$, which reads for its real part

$$\epsilon(\omega)\sim 1+\frac{\omega_p^2}{\overline{\omega_g}^2}, \tag{7}$$

where $\overline{\omega_g}$ is the average (Penn) gap of the solid[8] (which, for an anisotropic solid like a superlattice *depends also on polarization*), and $\omega_p=4\pi N_v$ is the plasma frequency of the valence electrons with density N_v. Although the number of atoms per unit cell is increased for the different superlattices, the *centers of gravity* of the full valence and conduction bands are preserved. The latter is true if the interaction between valence and conduction bands is negligible in the process of folding. The density of valence electrons per unit cell is the same for all the structures. Therefore, one expects the different well widths to have a similar Penn-gap contribution to the birefringence.

Finally, we are left with the influence of local fields. It is worth noting at this stage that the simple estimate given by Eq. (1) using the index of refraction of bulk GaAs and AlAs gives $\sim$0.04. This is a very large value for typical birefringences and could account, in fact, for most of the measured Δn_{bg}. In addition, this large contribution of the local fields illustrates the importance of the effect in layered structures. Nazarov[20] has demonstrated that Eq. (1) is valid for layered structures in the limit of $a \ll$ MQW period $\ll\lambda$, where a is the bulk lattice parameter. In the limit where the MQW period $\sim a \ll \lambda$, a new *bulk-like* material is created. In this case these relations should not hold, and the local-field correction should decrease to the small typical values found in bulk semiconductors. This change should, accordingly, be of the order of $\sim$0.04, which is, in fact, what is observed in Fig. 5(c) for Δn_{bg}. For structures with MQW period $\gg\lambda$, on the other hand, light propagates as in a homogeneous material and hence the local-field corrections should also recover the small values typical of bulk GaAs and AlAs. Thus, the limit considered by Nazarov[20] represents a maximum in the local-field corrections to the birefringence of layered media. Unfortunately, we are not able to explore by transmission measurements in waveguided MQW's the birefringence of

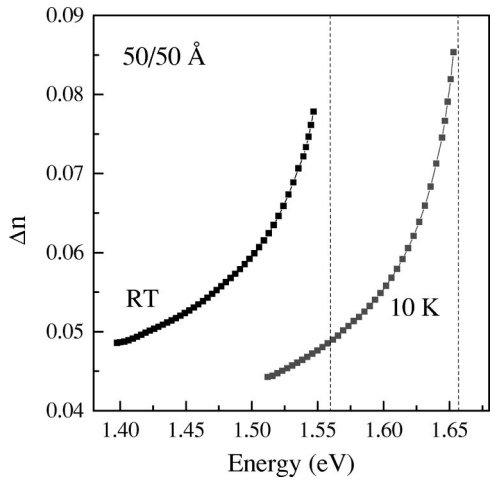

FIG. 6. Birefringence dispersion in the 50/50-Å structure at two different temperatures: 10 K and RT. The temperature-induced shift of the electronic gap upon cooling manifests itself as a shift towards high energies in the dispersion of the birefringence.

structures with periods larger than 70 Å due to the narrow window defined by the MQW's and GaAs substrate absorption gaps. The above handwaving arguments concerning local-field corrections can also be stated within a formal microscopic theory. As we mentioned in the Introduction, in order to take into account the local-field effects, an infinite matrix ought to be inverted. The local fields come into play through the off-diagonal elements of this matrix, which are dielectric functions evaluated at reciprocal lattice vectors $\vec{G} \neq 0$. The limit of small periods is equivalent to the limit of large $\vec{G}$'s. Bechstedt *et al.*[21] have demonstrated that the wave vector-dependent dielectric susceptibility rapidly decreases with increasing $\vec{G}$'s. We believe that the results in Fig. 5(c) clearly indicate that local fields are a predominant contribution to the background birefringence of MQW's.

B. Temperature dependence of $\Delta n(\omega)$

In order to further understand the effect of the proximity of the gap on the dispersion, the low-temperature birefringence was measured for the 50/50 sample. To extend the room-temperature calibration for Δn^0, we followed the temperature-induced shift of the spectral position for certain fringes during the cooling process and used the simple relation: $\Delta n/\lambda = \text{const}(T)$ to obtain a new calibration. In the light of the intrinsic accuracy of the method, we neglected the cooling-induced compression of the sample. Figure 6 shows two curves for $\Delta n(\omega)$ taken at 10 and 300 K. The modifications in $\Delta n(\omega)$ can be attributed to the temperature-induced shift of the fundamental gap. Furthermore, at 10 K data can be obtained closer to the gap than at RT due to the sharper absorption threshold at low temperatures. In this sense, note that the dispersion data come closer to the gap (displayed with a dashed vertical line as in Fig. 4) at 10 K. Most of the features of the temperature change in Δn can be easily understood but, in addition, a puzzling result arises. As mentioned before, the fact that the singularity in the dispersion shifts to higher energies can be ascribed to the blueshift of the direct gap at low temperatures. This shift of the resonance can be used, in fact, as an experimental demonstration that the dispersion comes from a given gap. Actually, this effect will be used later to demonstrate that the dispersion of the birefringence in the QD structures is produced by the InP dots. A simple fit of the data in Fig. 6 with the analytic model of Eq. (6) reveals that Δn_{gap} increases by $\sim 15\%$ from RT to 10 K, as one would expect from a stronger excitonic transition at low temperatures. However, the background birefringence Δn_{bg} is seen to decrease by $\sim 30\%$ from RT to 10 K. Since the average Penn gap is expected to blueshift as the temperature is lowered, a decrease of Δn_{bg} can be naturally expected. Nonetheless, this shift is much too large to be solely attributed to the temperature-induced blueshift of the average Penn gap. We believe that transitions to confined states within the wells other that the first hh and lh subbands, must be explicitly separated from the Penn-gap contribution and properly treated in order to understand this effect. Further work needs to be done in order to clarify this specific point.

C. Dimensionality dependence of $\Delta n(\omega)$

In addition to the effect of temperature, we highlight the influence of the dimensionality of the JDOS in the birefringence of microstructures and, to this end, we shall illustrate the example of an InP QD structure. In this sample, the average thickness (~ 15 Å) of the QD layer is much smaller than the thickness of the matrix. At first glance, a weak contribution to the birefringence should be expected from the single layer of InP-QD's. In Fig. 7(a) we show the dispersion of the in-plane birefringence at RT and 12 K for this sample. The data followed from the cross-polarization transmissions shown in Figs. 7(b) and 7(c), where the respective PL emissions from the front surface are also displayed (as in Fig. 1 for the MQW's). The PL spectra clearly demonstrate a blueshift produced by the temperature dependence of the gap together with a peak narrowing, as expected. As in the case of the MQW's, we followed the position of one fringe as a function of temperature to obtain Δn^0 at low temperatures. The temperature-induced shift of the fringe position can be observed in Fig. 7(d) together with a fit given by $\hbar\omega_0(T) = \hbar\omega_0(0) - cT^2/(T+\Theta)$, where $\hbar\omega_0(0) = 1.6813$ eV, $c = 5.4\times 10^{-4}$ eV/K, and $\Theta = 240$ K. This law is the same as the well-known temperature dependence of the fundamental gap in semiconductors.[22] In the spectral range closer to the gap of the dots the birefringence increases from 0.02 up to 0.028 (i.e., $\sim 40\%$). The temperature dependence shown in Fig. 7(a) implies that the dispersion is caused by the QD gaps. Note that the contribution of the QD-electronic states to the resonant birefringence is relatively stronger than that in the case of the MQW's, especially considering that the ratio of the QD-layer thickness to the thickness of the matrix is about 10^{-2}. This stronger resonance effect can be easily explained by a change in the effective dimensionality of the JDOS from 2D in MQW's to zero dimensions (0D) in QD's, respectively. The data in Fig. 7(a) are extremely well reproduced by a birefringence of the form

$$\Delta n(\omega) = \Delta n_{bg} + \Delta n_{gap}\left[\frac{1}{1-\omega/\omega_g}\right], \tag{8}$$

which is the equivalent of Eq. (6) for a 0D-JDOS. Moreover, the fits yield $\Delta n_{bg} \sim 0.018$ while $\Delta_{gap} \sim 0.001$, showing that

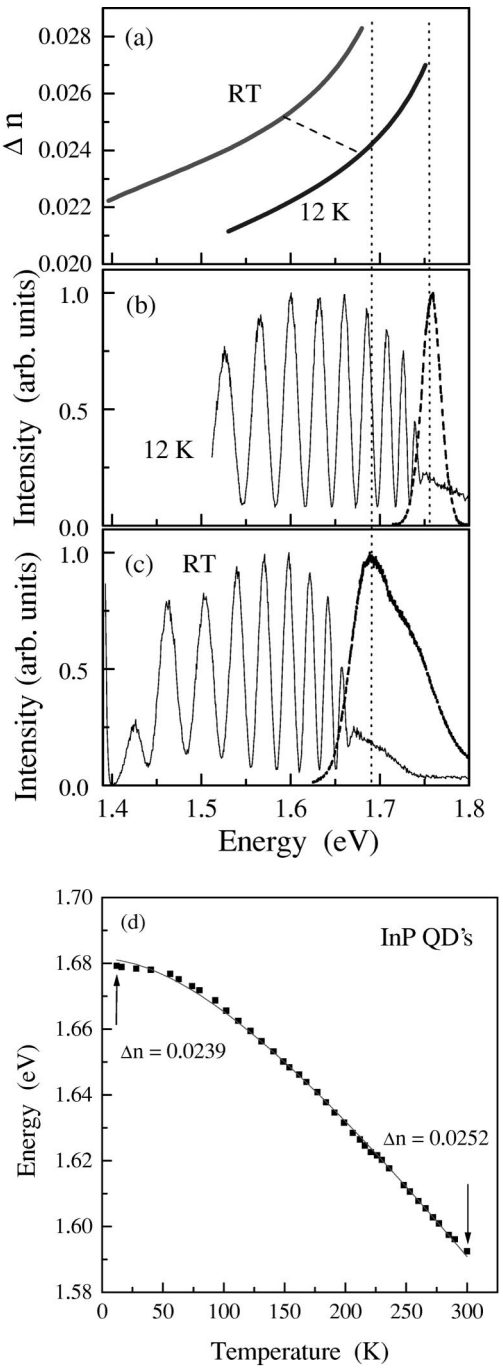

FIG. 7. (a) Birefringence in the waveguide structure with a single layer of InP QD's at 12 K and RT. The resonant part of the curve shifts with the cooling-induced increase of the fundamental gap of the QD's. PL (dashed line) and transmission (solid line) spectra of the same structure at 12 K and RT are shown in (b) and (c), respectively. In (d) we show the temperature-induced shift of a fringe located at 1.592 eV at RT [shown schematically in (a) with a dashed line]. The solid line represents a fit: $\hbar\omega_0(T)=\hbar\omega_0(0)-cT^2/(T+\Theta)$. See the text for details.

the main contribution to the birefringence in the transparency region comes from the background, except close to the gap where the strong resonance accounts for an increase of $\sim 40\%$ in Δn. In the particular case of the QD's, several different sources could account for a measurable background birefringence. First, the dots are asymmetric as explained in Sec. II. This asymmetry can induce different confinements and a different coupling for polarizations along the planes or the $\hat{z}$ axis, respectively. Second, the InP dots are under stress in the $In_{0.48}Ga_{0.52}P$ matrix, leading to an additional anisotropy source.[9] Third, the $In_{0.48}Ga_{0.52}P$ matrix is also strained close to the dots, so that a contribution from the matrix itself to the observed background birefringence could be expected. Finally, a measurable waveguiding effect may be present in this sample as compared to the MQW's. Note that the thickness of the matrix ($0.13\,\mu$m) is comparable with the wavelength of the transmitted light. Even if the material inside a planar waveguide is isotropic, as soon as the thickness along $\hat{z}$ is of the order of λ, a sizable birefringence is generated according to the different boundary conditions of the electric field of the light for polarizations parallel or perpendicular to $\hat{z}$, as explained before. This birefringence is not *intrinsic* of the material but rather depends on the geometry of the waveguide.[7] Provided that the material inside the waveguide is birefringent, the boundary conditions produce an effect which is added to the intrinsic one. This birefringence is minimized if the waveguide is thick enough, but may be playing a role in the value of Δn_{bg} for the QD structure. In any case, the experimental data of Fig. 7(a), and their theoretical interpretation in terms of Eq. (8), clearly show that the leading term in the dispersion of the birefringence close to the gap is the strong resonance enhancement brought forth by the reduced dimensionality of the JDOS in the QD's. We believe that the stronger resonance enhancement expected in 0D [Eq. (8)] as compared to 2D [Eq. (6)] is readily seen in these results and highlights the importance of the effective dimensionality of the JDOS for optical transitions.

D. Fabry-Perot determination of $n_{\parallel,\perp}(\omega)$

Finally, we comment on the application of Fabry-Perot interferences to the determination of the optical constants below the gap. The transmission technique can be used not only for the measurement of the difference between $n_{\parallel}$ and $n_{\perp}$ but also for the estimation of their absolute values. It has been demonstrated in Ref. 7 that transmission spectra between parallel polarizers in MQW's display *Fabry-Perot oscillations*. These are better observed if coherent (laser) light is used instead of a white light source. Spectra obtained for the 50/50 sample with a Ti-sapphire laser are shown in Fig. 8(a). The following expression [similar to Eq. (2)] determines the position of the maxima of the Fabry-Perot fringes

$$2n_{\parallel,\perp}(\lambda)d=N_{\parallel,\perp}\lambda, \tag{9}$$

where $N_{\parallel,\perp}$ are integer numbers, and $\parallel$ or $\perp$ apply to incident and transmitted polarizations simultaneously parallel or perpendicular to $\hat{z}$, respectively. Note the additional factor of 2 in comparison with Eq. (2). Using a treatement similar to that used for the case of the birefringence, we obtain

$$n_{\parallel,\perp}(\omega)=\frac{1}{\omega}\left[n^0_{\parallel,\perp}\omega_0+\frac{\pi c}{d}\int_{\omega_0}^{\omega}\frac{1}{\Delta\omega'_{\parallel,\perp}(x)}dx\right], \tag{10}$$

where the meanings of the parameters are the same as in Eq. (4). Figure 8(b) shows the experimental dependences of the distance between Fabry-Perot oscillations $\Delta\omega'_{\parallel,\perp}(\omega)$ in the

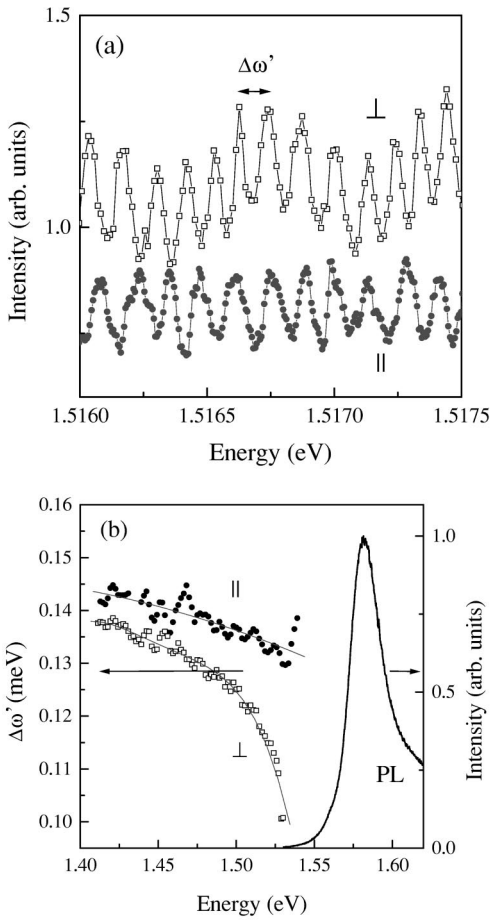

FIG. 8. (a) Transmission spectra between parallel polarizers either $\perp$ or $\parallel$ to $\hat{z}$ in the 50/50 structure at RT. (b) Distance between peaks of the Fabry-Perot oscillations ($\Delta\omega'$) for the data in (a) and the PL spectrum of this structure, which shows the position of the fundamental gap.

50/50 structure with $d=1.15$ mm, together with the PL spectrum of the sample. The difference between these two functions, $\Delta\omega'_{\perp}<\Delta\omega'_{\parallel}$, confirms that the sign of the birefringence has been determined correctly. A calibration value of $n_{\perp}=3.24$ at $\hbar\omega=1.476$ eV, which is close to that from Ref. 2, has been used for Eq. (10). This value was adjusted so that the difference between $n_{\parallel}$ and $n_{\perp}$ coincides with the measured birefringence $\Delta n(\omega)$ for this structure in the whole spectral range. The dispersion curves so obtained for $n_{\parallel,\perp}$ are displayed in Fig. 9 and show, in fact, that it is possible to independently measure the two principal components of the dielectric tensor (not just their difference). The beauty of the result in Fig. 9 resides in that it clearly shows a stronger resonant dispersion for $n_{\perp}$ with respect to $n_{\parallel}$. Note that when the electric field of the light $\vec{E}$ is perpendicular to $\hat{z}$, the lowest gap to which it can couple is the hh-interband transition. If $\vec{E}\|\hat{z}$, on the other hand, the lowest gap is the lh-interband transition, which is at higher energies due to the hh-lh splitting. One expects, accordingly, to observe a stronger dispersion for $n_{\perp}$ close to the gap, thus revealing the different symmetries of the coupling for the two polarizations.

The method just described is significant for detailed investigations of light propagation in waveguide structures.

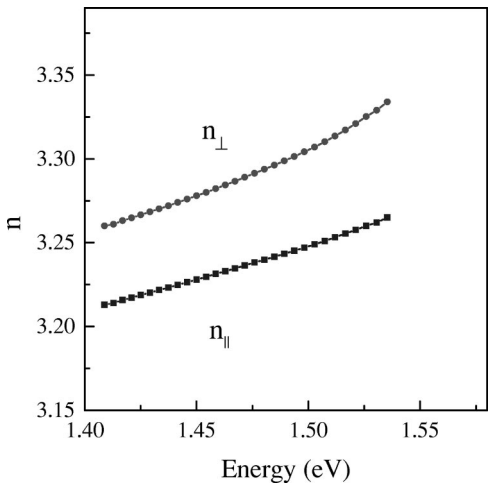

FIG. 9. Dispersion of the two components of the refractive index $n_{\parallel}$ and $n_{\perp}$ in the 50/50 structure obtained at RT from the Fabry-Perot oscillations in Fig. 8.

For example, with the help of Fig. 9 it is easy to determine which two orthogonally-polarized electromagnetic waves with different frequencies (ω_1 and ω_2) will propagate through the MQW's with the same velocity, thus fulfilling the phase-matching condition. This problem is relevant for the characterization of frequency converters, as we shall comment below.

IV. CONCLUSIONS

The linear optical birefringence has been studied in GaAs/AlAs MQW's using transmission spectroscopy. A significant change in the background birefringence for MQW's has been observed as a function of the period and attributed to the presence of local fields. We regard this evidence as the most important conclusion of this paper. Moreover, a comparatively strong resonant birefringence in the InP QD's has been observed and ascribed to the lower dimensionality of the dots with respect to the QW's. The effect of temperature as well as the exploitation of Fabry-Perot interferences to obtain absolute values for $n_{\parallel,\perp}$ have also been presented.

It is worth noting that the characterization of the birefringence in semiconductor microstructures is a subject of great practical interest at present. One of the most promising areas for potential applications of artificially constructed birefringent devices is the design of frequency converters. While the GaAs/AlAs system is recognized as an excellent candidate for third-order nonlinear optics, its application in second harmonic generation has been hampered by the lack of a sufficiently high birefringence to phase match the different waves. Very recently, Fiore *et al.*[23] demonstrated phase matching in a composite structure made of layers of GaAs and thin oxidized AlAs (Alox). Wet oxidation converts AlAs into an oxide with refractive index $n\simeq 1.6$ and increases the contrast with GaAs, making the birefringent phase matching for second harmonic generation possible. The enhanced index of refraction contrast of Alox with respect to GaAs also produced a breakthrough in the construction of Bragg reflec-

tors for MQW lasers and microcavities. Birefringent waveguides grown on novel substrate directions have also been proposed.[23] We hope that our work will contribute to the development of characterization methods for these devices as well as to the general understanding of one of the most basic optical properties of microstructures.

ACKNOWLEDGMENTS

The authors are grateful to P. Santos and B. Koopmans for useful discussions. This work has been partially supported by the Alexander von Humboldt Foundation and by U.S. DOE Grant No. DE-FG02-84ER45095.

[1] J. S. Weiner, D. S. Chemla, D. A. B. Miller, H. A. Baus, A. C. Gossard, W. Wiegmann, and C. A. Burrus, Appl. Phys. Lett. **47**, 664 (1985).

[2] R. Grousson, V. Voliotis, P. Lavallard, M. L. Roblin, and R. Planel, Semicond. Sci. Technol. **8**, 1217 (1993).

[3] V. Voliotis, R. Grousson, P. Lavallard, and R. Planel, Phys. Rev. B **52**, 10 725 (1995).

[4] M. Berz, R. Houdré, E. F. Steigmeier, and F. K. Reinhart, Solid State Commun. **86**, 43 (1993).

[5] K. Ogawa, T. Katsuyama, and H. Nakamura, Phys. Rev. Lett. **64**, 796 (1990).

[6] B. Koopmans, B. Richards, P. V. Santos, K. Eberl, and M. Cardona, Appl. Phys. Lett. **69**, 782 (1996).

[7] A. Fainstein, P. Etchegoin, P. V. Santos, M. Cardona, K. Tötemeyer, and K. Eberl, Phys. Rev. B **50**, 11 850 (1994).

[8] M. Cardona, in *Atomic Structure and Properties of Solids*, edited by E. Burstein (Academic Press, New York, 1972), p. 513.

[9] P. Etchegoin, A. Fainstein, A. A. Sirenko, B. Koopmans, B. Richards, P. V. Santos, M. Cardona, K. Tötemeyer, and K. Eberl, Phys. Rev. B **53**, 13 662 (1996).

[10] Note that this is not strictly true if the wave vector of the light comes into play. In this case, a small birefringence quadratic in $\vec{k}$ appears. See P. Yu and M. Cardona, Solid State Commun. **9**, 1421 (1971), for further details.

[11] N. Wiser, Phys. Rev. **129**, 62 (1963); A. L. Adler, *ibid.* **126**, 413 (1962).

[12] M. Cardona, in *Semiconductor Superlattices and Interfaces*, Proceedings of the International School of Physics ''Enrico Fermi,'' Course CXVII, Varena on Lake Como, Villa Monastero, 1991, edited by A. Stella and L. Miglio (North-Holland, Amsterdam, 1993), p. 435.

[13] M. Cardona, J. Electron. Mater. **22**, 27 (1993).

[14] A. Kurtenbach, K. Eberl, and T. Shitara, Appl. Phys. Lett. **66**, 361 (1995).

[15] M. K. Zundel, P. Specht, K. Eberl, N. Y. Jin-Phillipp, and F. Phillipp, Appl. Phys. Lett. **71**, 2972 (1997).

[16] A. A. Sirenko, M. K. Zundel, T. Ruf, K. Eberl, and M. Cardona, Phys. Rev. B **58**, 12 633 (1998).

[17] T. S. Moss, G. J. Burrel, and B. Ellis, *Semiconductor Optoelectronics* (Butterworth, London, 1973).

[18] G. Danan, B. Etienne, F. Mollot, R. Planel, A. M. Jean-Louis, F. Alexandre, B. Jusserand, G. Le Roux, J. Y. Marzin, H. Savary, and B. Sermage, Phys. Rev. B **35**, 6207 (1987).

[19] C. W. Higginbotham, M. Cardona, and F. H. Pollak, Phys. Rev. **184**, 821 (1969).

[20] V. U. Nazarov, Phys. Rev. B **49**, 17 342 (1994).

[21] F. Bechstedt, M. Fiedler, C. Kress, and R. Del Sole, Solid State Commun. **89**, 669 (1994).

[22] Y. P. Varshni, Physica (Amsterdam) **34**, 149 (1967).

[23] A. Fiore, V. Berger, E. Rosencher, P. Bravetti, and J. Nagle, Nature (London) **391**, 463 (1998); A. Fiore, V. Berger, E. Rosencher, S. Crouzy, N. Laurent, and J. Nagle, Appl. Phys. Lett. **71**, 2587 (1997).